Twinning and Dislocation Evolution during Shock Compression and Release of Single Crystals: Real-Time X-Ray Diffraction

Stefan J. Turneaure, P. Renganathan, J. M. Winey, and Y. M. Gupta

Phys. Rev. Lett. **120**, 265503 — Published 29 June 2018

DOI: 10.1103/PhysRevLett.120.265503

Twinning and dislocation evolution during shock compression and release of single crystals: real-time, x-ray diffraction

Stefan J. Turneaure[1], P. Renganathan[1], J. M. Winey[1] and Y. M. Gupta[1,2]

[1]Institute for Shock Physics and [2]Department of Physics and Astronomy, Washington State University, Pullman, Washington 99164, USA

Abstract

Determining the temporal evolution of twinning and/or dislocation slip, in real time (nanoseconds), in single crystals subjected to plane shock wave loading is a long-standing scientific need. Non-cubic crystals pose special challenges because they have many competing slip and twinning systems. Here, we report on time-resolved, *in situ*, synchrotron Laue x-ray diffraction measurements during shock compression and release of magnesium single crystals that are subjected to compression along the *c*-axis. Significant twinning was observed directly during stress release following shock compression; during compression, only dislocation slip was observed. Our measurements unambiguously distinguish between twinning and dislocation slip on nanosecond timescales in a shocked hexagonal-close-packed metal.

PACS numbers: 62.50.Ef, 62.20.F-, 81.05.Bx, 81.70.Bt

Plane shock wave experiments are ideally suited to study, in real-time, material deformation phenomena at high stresses and high-loading rates, commonly encountered in high-velocity impacts and explosions. Studies on single crystals are particularly valuable for examining fundamental mechanisms, e.g. dislocation slip and/or twinning, that govern plastic deformation under shock wave loading because complications arising due to grain boundary effects are avoided [1-3]. In addition, shock wave propagation along different crystal axes can be used to examine the role of crystal anisotropy under well-characterized loading conditions, and to explore how different dislocation and twinning systems can be selectively activated and examined [3-5]. The latter feature is particularly valuable for understanding deformation mechanisms in non-cubic crystals, because a large number of slip and twinning systems can be operational in such crystals [5,6]. Separating and understanding the role of dislocation slip and twinning mechanisms in shock wave induced plastic deformation in single crystals is of fundamental importance for developing accurate material models [3,5,6].

Although plane shock wave studies in single crystals have been carried out for nearly five decades, real-time examination (nanosecond time scales) of deformation mechanisms at the microscopic level during shock loading has been lacking in such studies. The single crystal studies to date have focused on shock wave profile measurements (continuum results) (e.g. see Refs. 1-5,7,8) and/or microstructural examination of samples recovered well after the shock event (e.g. see Refs. 9-12).

As valuable as the above two types of experiments have been for examining elastic-plastic deformation in shocked single crystals, the lack of real-time, microscopic measurements makes it difficult to establish the specific micromechanisms operative during shock compression

and release, while the sample is in the well-characterized uniaxial strain state. The challenging nature of the desired measurements has been a significant scientific hurdle.

To address the long-term scientific challenge indicated above, we have successfully carried out real-time x-ray diffraction (XRD) measurements – using synchrotron x-rays coupled to plate impact experiments at the recently developed Dynamic Compression Sector (Advanced Photon Source, Argonne, IL) – to examine the temporal evolution of deformation mechanisms in magnesium (Mg) single crystals subjected to shock compression and release along the *c*-axis. We report on the direct and unambiguous observation of deformation twinning only during release following plane shock wave compression. During compression, only dislocation slip was observed.

Figure 1A shows the configuration used for simultaneous multi-frame Laue XRD and wave profile measurements on shock-compressed Mg single crystals [13]. A flat-faced polycarbonate projectile impacted a Mg crystal along the *c*-axis resulting in a planar shock wave propagating through the Mg crystal; when the shock wave reached the Mg free surface, it reflected as a stress release wave. Four XRD patterns (~100 ps duration; 153.4 ns between frames) were recorded over several hundred nanoseconds using broadband x-rays (see Figs. S1 and S2 [13]). This combination of plate impact and time-resolved XRD capabilities allowed us to examine the active deformation mechanisms during both shock compression and release in a single experiment. In contrast, time-resolved XRD measurements during both shock-compression and release in a single experiment are not possible using current laser compression x-ray diffraction capabilities [14-16].

Five plate impact experiments incorporating XRD and wave profile measurements were performed with peak stresses from 2.8-6.1 GPa. Table S1 [13] lists Mg sample parameters and

Table S2 [13] lists the experimental details including projectile velocities, XRD frame times relative to impact, and sample to x-ray detector distances. Here we focus on the results of one plate impact experiment with an impact stress of 5.85 GPa; results for the other four experiments are similar and are provided in the Supplemental Materials [13].

Figure 1B shows a representative Laue XRD pattern from a Mg single crystal at ambient conditions; the indexed Laue XRD spots provide the precise crystal orientation.

To accurately link the XRD measurements and the continuum response temporally, a velocity interferometer system for any reflector (VISAR) [17] was used to record the velocity history of the Mg rear surface. A representative free surface velocity history is shown in Fig. 1C. The wave profile features in Fig. 1C are similar to those observed previously in Mg single crystals shock-compressed along the *c*-axis [18,19].

Quasi-static experiments have shown that both dislocation slip and twinning are important deformation mechanisms for Mg [6,20]. Because of the high stresses, high loading rates, and short timescales associated with shock wave compression, the relative importance of the various dislocation slip and deformation twin systems in shock experiments cannot be inferred from quasi-static results. However, the deformation mechanisms observed under quasi-static loading provide an excellent starting point for discussing deformation mechanisms operative under shock compression and/or release.

Shock compression along the Mg *c*-axis, due to the hexagonal symmetry of Mg, does not activate basal, prismatic, and pyramidal <**a**> dislocation slip; these systems experience no resolved shear stress for *c*-axis loading [2,20]. However, pyramidal <**c**+**a**> slip provides a possible mechanism for shock compression and release along the *c*-axis [2,6,21]. Unlike dislocation slip, deformation twinning is sensitive to the sign of the shear stress and different

twin types are possible during shock compression (where longitudinal stress > lateral stress) and during release (when lateral stress > longitudinal stress). For shock compression along the Mg *c*-axis, $\{10\bar{1}1\}<\bar{1}012>$ contraction twins [6] and double twins ($\{10\bar{1}2\}<\bar{1}011>$ extension twins formed within contraction twins) [22] are possible. During stress release, $\{10\bar{1}2\}<\bar{1}011>$ extension twins [6] are possible. These different deformation mechanisms cited were used to analyze and interpret the XRD patterns measured in the present experiments.

XRD patterns from the 5.85 GPa experiment are shown in Figs. 2A-2D. The diffraction pattern in Fig. 2A, taken just prior to impact, matches the ambient pattern in Fig. 1B, as expected. The diffraction pattern in Fig. 2B was obtained 110 ns after impact while elastic and plastic shock waves were propagating towards the rear surface of the Mg sample (see Fig. 2E). The Laue diffraction spots observed here are the same as those observed in the diffraction pattern obtained before impact (Fig. 2A), but the spots for shocked Mg are significantly elongated. The diffraction patterns in Figs. 2C and 2D were obtained after the plastic shock wave reflected as a release wave from the Mg free surface (see Figs. 2F and 2G). A significant number of new Laue spots are apparent in these diffraction patterns, indicating large changes in the Mg crystal orientation. Similar results were obtained from the four additional plate impact XRD experiments (see Figs. S3-S6).

To relate the XRD measurements to the loading history, numerical simulations were used to determine the continuum variables for the shocked Mg single crystals. Free surface velocity histories were calculated using a continuum modeling framework developed previously for hexagonal-close-packed single crystals [3], and subsequently used to model measured shock wave profiles in Mg single crystals [19,23]. As shown in Figs. 1C and S7, the simulations provide a good match to the measured velocity histories for all experiments. Because of the

good match between the measured and simulated Mg free surface velocity histories, the simulations were used to determine the stresses and densities in our experiments and the same are listed in Table S3. The calculated longitudinal stress snapshots at times corresponding to the recorded XRD patterns are shown in Figs. 2E-2G and in Figs. S8-S11.

To gain insight into the deformation mechanisms active during shock compression and release, XRD simulations incorporating crystallographic changes due to various deformation mechanisms were carried out and compared with the measured XRD patterns [13]. The Mg lattice parameters (*a* and *c*) used in the XRD simulations were obtained from the calculated stresses (Table S3) and finite strain elasticity theory [24,25] incorporating elastic constants up to fourth order [26,27]. The XRD simulations incorporated a distribution of random micro lattice rotations (described later in the paper) with a maximum rotation of 2^{o} to account for the observed Laue spot elongation. The orientation of the Mg lattice in extension (contraction) twins is determined by a rotation of the *c*-axis by $\pm 86.3^{o}$ (56.2^{o}) around the three independent $\langle 11\bar{2}0 \rangle$ axes, resulting in six twin variants (different Mg lattice orientations) for both contraction and extension twins. XRD simulations, incorporating deformation twinning, assumed equal volume fractions for each of the six equivalent twin variants. The simulated intensities of the Laue spots from the twin variants and from the untwinned fraction of the Mg crystal were proportional to the corresponding volume fractions.

An XRD simulation incorporating contraction twinning during shock compression results in many new simulated Laue XRD spots (see Fig. S12) that are not observed in the XRD measurements in the shock compressed state (Fig. 2B), demonstrating that contraction twins (and therefore also double twins) are not activated during shock compression of Mg along the *c*-axis for stresses reaching 6 GPa. Hence, we conclude that plastic deformation during shock

compression of Mg along the *c*-axis from 3-6 GPa is dominated by dislocation slip, likely involving pyramidal <**c**+**a**> dislocations [21].

In contrast to the XRD pattern observed in the shock-compressed state (Fig. 2B), the diffraction patterns in the released states (Figs. 2C and 2D) contain many new Laue spots, consistent with deformation twinning. XRD simulations incorporating $\{10\bar{1}2\}<\bar{1}011>$ extension twins are shown in Figs. 2I and 2J, corresponding to the XRD patterns measured after the onset of stress release 263 ns and 417 ns after impact, respectively. The twin volume fractions used in the XRD simulations were determined from the continuum simulations and are listed in Table S3. The diffraction simulations incorporating extension twinning match the Laue spots observed after the onset of stress release, providing direct and unambiguous proof that significant extension twinning occurs during release. Similar good agreement between XRD patterns measured after stress release and XRD simulations incorporating extension twinning was also found for the other four experiments (see Figs. S13-S16).

A common feature of all the Laue XRD patterns measured after shock compression and after release is a significant elongation of the Laue spots relative to the ambient spots. The observed Laue spot broadening can be caused by deviatoric elastic lattice strain distributions (related to local strength) or by lattice rotation distributions (mosaic spread). XRD simulations incorporating physically reasonable deviatoric elastic strains do not cause significant Laue spot broadening (see Fig. S17), leading to the conclusion that the observed Laue spot broadening is primarily due to a small distribution of lattice rotations [13]. Indeed, all of the XRD simulations incorporating random lattice rotations with a maximum rotation of 2 degrees provide a good match to the measured XRD spot sizes. Observation of Laue spot elongation after shock compression, but before twinning has occurred, demonstrates that dislocation slip in shocked Mg

single crystals results in crystal mosaic spread. Because the mosaic spread in the released state is nearly the same as in the shock compressed state, it can be concluded that dislocation slip is quite limited during release. Hence, extension twinning dominates the release response, resulting in little, if any, additional mosaic spread.

The XRD results presented here for shock compression and release of Mg single crystals along the *c*-axis can be understood in terms of the resolved shear stresses that appear on different dislocation slip or deformation twinning systems. Because the resolved shear stresses appearing on pyramidal slip systems are similar to those on contraction twinning systems for *c*-axis compression (see Table S4), the dominant role of dislocation slip in the plastic deformation of Mg single crystals shock-compressed along the *c*-axis suggests that the resolved shear stress required to activate pyramidal slip is significantly lower than that required to activate contraction twinning. In contrast, the resolved shear stress required to activate extension twinning in Mg single crystals was shown to be significantly lower than that required to activate pyramidal slip in quasi-static loading experiments [20]. Although extension twinning cannot operate during compression in Mg single crystals shocked along the *c*-axis due to crystallographic constraints [6,28], during release the resolved shear stress for extension twinning changes sign. This change, in turn, causes extension twinning to be activated and to become the dominant plastic deformation mechanism during release. While the present experiments differ significantly from quasi-static experiments in terms of loading rate and duration, loading path (uniaxial strain versus uniaxial stress), and peak stresses attained, the micromechanisms indicated above are consistent with those observed under quasi-static loading [6, 21].

The time-resolved Laue x-ray diffraction (XRD) experiments and results presented here have provided the first direct, *in situ* observation of the active deformation mechanisms in shock

compressed and released single crystals. The roles of dislocation slip and deformation twinning have been directly and unambiguously distinguished – on nanosecond time scales – in Mg single crystals during shock compression and release along the *c*-axis. Laue XRD measurements in future experiments that examine different Mg crystal orientations will provide additional insight into the micromechanisms governing inelastic deformation in Mg single crystals during shock wave compression/release.

The experimental approach presented here has addressed the long-standing need for real-time, *in situ* measurements to establish the specific micromechanisms operative in single crystals during plane shock wave loading. A key element of this approach is the acquisition of time-resolved XRD measurements during both shock compression and release in a single experiment. The insights gained from such experiments are crucial, not only for identifying micromechanisms, but also for understanding how these mechanisms relate to the corresponding continuum response – an essential step for linking material response at different length scales. The experimental approach presented here is well-suited for providing such insights for a wide range of important materials, including hexagonal-close-packed metals and body-centered cubic metals, for which dislocation slip and deformation twinning are competing inelastic deformation mechanisms under shock wave compression and release.

Acknowledgments

Yoshi Toyoda, Travis Volz, Paulo Rigg and the DCS staff are thanked for assistance with the plate impact experiments. Jeff Klug provided the calculated spectral flux. This publication is based upon work supported by the U.S. Department of Energy (DOE), National Nuclear Security Administration (NNSA) under Award Number DE-NA0002007. This publication is also based upon work performed at the Dynamic Compression Sector supported by the DOE/NNSA under Award Number DE-NA0002442 and operated by Washington State University. This research used resources of the Advanced Photon Source, a DOE Office of Science User Facility operated for the DOE Office of Science by Argonne National Laboratory under Contract No. DE-AC02-06CH11357.

List of References

1. O. E. Jones and J. D. Mote, J. Appl. Phys. **40**, 4920 (1969).
2. J. N. Johnson, O. E. Jones and T. E. Michaels, J. Appl. Phys. **41**, 2330 (1970).
3. J. M. Winey and Y. M. Gupta, J. Appl. Phys. **116**, 033505 (2014).
4. W. J. Murri and G. D. Anderson, J. Appl. Phys. **41**, 3521 (1970).
5. L. E. Pope and J. N. Johnson, J. Appl. Phys. **46**, 720 (1975).
6. M. H. Yoo, Met. Trans. A **12**, 409 (1981).
7. J. R. Asay, G. R. Fowles, G. E. Duvall, M. H. Miles and R. F. Tinder, J. App. Phys. **43**, 2132 (1972).
8. H. Huang and J. R. Asay, J. Appl. Phys. **101**, 063550 (2007).
9. M. A. Mogilevskiy, Phys. Metals Metall. **28**, 130 (1969).
10. P. S. Follansbee and G. T. Gray III, Int. J. Plast. **7**, 651 (1991).
11. J. N. Florando, N. R. Barton, B. S. El-Dasher, J. M. McNaney, M. Kumar, J. Appl. Phys. **113**, 083522 (2013).
12. N. Dixit, L. Farbeniec, K. T. Ramesh, Mater. Sci. Eng. A **693**, 22 (2017).
13. See Supplemental Material at […] for additional experimental details and results, continuum simulation details and XRD simulation details
14. M. J. Suggit et al., Nat. Commun. **3**, 1224 (2012).
15. A. J. Comley et al., Phys. Rev. Lett. **110**, 115501 (2013).
16. C. E. Wehrenberg et al., Nature **550**, 496 (2017).
17. L. M. Barker and R. E. Hollenbach, J. Appl. Phys. **43**, 4669 (1972).
18. G. I. Kanel et al., J. Appl. Phys. **116**, 143504 (2014).
19. J. M. Winey, P. Renganathan and Y. M. Gupta, J. Appl. Phys. **117**, 105903 (2015).

20. E. W. Kelley and W. F. Hosford Jr., Trans. Met. Soc. AIME **242**, 5 (1968).

21. K. Y. Xie, Z. Alam, A. Caffee and K. J. Hemker, Scr. Mater. **112**, 75 (2016).

22. W. H. Hartt and R. E. Reed-Hill, T. Metall. Soc. AIME **242**, 1127 (1968).

23. P. Renganathan, J. M. Winey and Y. M. Gupta, J. Appl. Phys. **121**, 035901 (2017).

24. D. C. Wallace, in *Solid State Physics*, edited by H. Ehrenreich, R. Seitz, D. Turnbull, (Academic, New York, 1970), Vol. 25, p. 301.

25. R. N. Thurston, in *Physical Acoustics: Principles and Methods*, edited by W. P. Mason, (Academic, New York, 1964), Vol. 1, Part A, p. 1.

26. E. R. Naimon, Phys. Rev. B **4**, 4291 (1971).

27. R. R. Rao and A. Padmaja, J. Appl. Phys. **67**, 227 (1990).

28. M. V. Klassen-Neklyudova, *Mechanical Twinning of Crystals* (Consultants Bureau, New York, 1964).

29. D. Errandonea, Y. Meng, D. Hausermann and T. Uchida, J. Phys. Condens. Matter **15**, 1277 (2003).

Figure Captions

1. (Color online) Experimental configuration for *in situ*, time resolved, x-ray diffraction and wave profile measurements on shock-compressed and released Mg single crystals compressed along the *c*-axis. (A) Flat-faced 12.7 mm diameter polycarbonate impactors, accelerated to 900-1800 m/s velocities using a powder gun, impacted 0.9 mm thick Mg crystals. Upon impact, elastic and plastic shock waves propagate through the Mg samples. About 150 ns after impact, the shock waves reach the Mg free surface and reflect as stress release waves. Broadband synchrotron x-ray pulses (~100 ps duration) were used to record four Laue x-ray diffraction patterns (153.4 ns between patterns) during shock-compression and during stress release providing direct insight into the operative deformation mechanisms (dislocation slip or twinning). Time-resolved continuum response was obtained by measuring the Mg free surface velocity using a velocity interferometer. (B) Ambient Laue x-ray diffraction image for a Mg single crystal sample prior to shock compression to 5.85 GPa. (C) Measured and simulated Mg free surface velocity history for a Mg sample shock-compressed along the *c*-axis to 5.85 GPa.
2. Measured and simulated x-ray diffraction patterns and corresponding stress snapshots from a representative plate impact experiment on a Mg single crystal shock compressed to 5.85 GPa along the *c*-axis and released. (A) Single pulse XRD pattern obtained 43 ns before impact showing ambient Laue XRD spots for the Mg single crystal and a diffuse inner ring due to the polycarbonate impactor. (**B**) Single pulse XRD pattern obtained 110 ns after impact while the shock waves are propagating through the Mg showing significant Laue spot elongation. (**C,D**) Single pulse XRD patterns obtained after the elastic and plastic shock waves reflected from the Mg free surface (263 ns and 417 ns

after impact, respectively) resulting in stress release. The same set of new Laue XRD spots (due to twinned regions of the Mg crystal) is observed in panels C and D. (**E-G**) Simulated stress snapshots corresponding to the times at which the XRD patterns were recorded. Blue arrows show direction of wave propagation. The center of the plastic shock wave reaches the Mg free surface 160 ns after impact. The twin volume fractions used in the XRD simulations are listed. (**H**) Simulated x-ray diffraction pattern corresponding to the XRD pattern recorded 110 ns after impact. The simulation is for a mosaic Mg crystal with a small distribution of random lattice rotations including rotations up to 2 degrees from the ambient crystal orientation. The random lattice rotations included in the XRD simulation explain the observed Laue spot elongation observed in panel B. (**I,J**) Simulated XRD patterns including small distribution of random lattice rotations (up to 2 degrees) for both the ambient Mg orientation and for the six extension twin variants corresponding to XRD patterns recorded 263 ns and 417 ns after impact, respectively. Simulated Laue XRD spots from the six extension twin variants match the new Laue spots observed after stress release. (**K**) Schematic showing loading direction, ambient Mg lattice, and one of the Mg extension twin variant orientations.

Figure 1

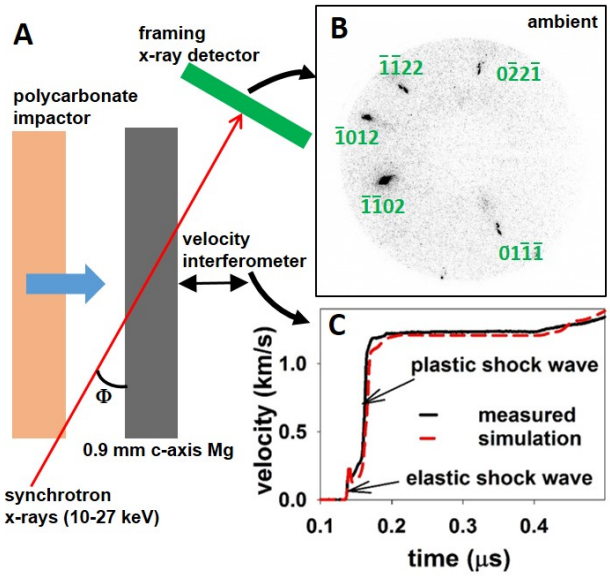
A
framing
x-ray detector
polycarbonate
impactor
velocity
interferometer
Φ
0.9 mm c-axis Mg
synchrotron
x-rays (10-27 keV)
B
ambient
$\bar{1}\bar{1}22$
$0\bar{2}2\bar{1}$
$\bar{1}012$
$\bar{1}\bar{1}02$
$01\bar{1}\bar{1}$
C
plastic shock wave
measured
simulation
elastic shock wave
velocity (km/s)
1.0
0.5
0.0
0.1
0.2
0.3
0.4
time (μs)

Figure 2

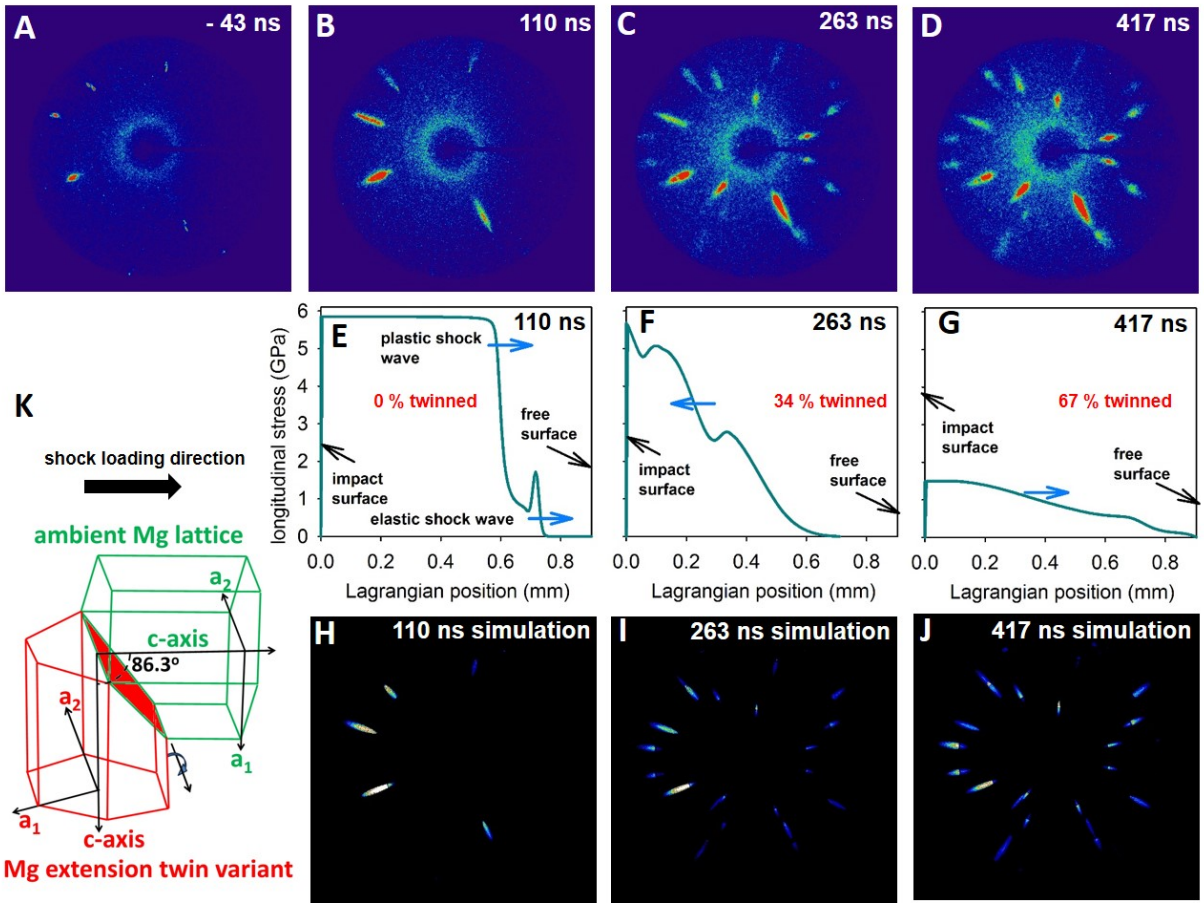
A
- 43 ns
B
110 ns
C
263 ns
D
417 ns
E
110 ns
plastic shock wave
0 % twinned
free surface
impact surface
elastic shock wave
F
263 ns
34 % twinned
impact surface
free surface
G
417 ns
67 % twinned
impact surface
free surface
longitudinal stress (GPa)
Lagrangian position (mm)
K
shock loading direction
ambient Mg lattice
c-axis
86.3°
Mg extension twin variant
H
110 ns simulation
I
263 ns simulation
J
417 ns simulation